

# The emergent dynamics of double-folded randomly branching ring polymers

Elham Ghobadpour,<sup>1,2,3</sup> Max Kolb,<sup>3</sup> Ivan Junier,<sup>1</sup> and Ralf Everaers<sup>4,3,\*</sup>

<sup>1</sup>*CNRS, UMR 5525, VetAgro Sup, Grenoble INP, TIMC, Université Grenoble Alpes, Grenoble, France*

<sup>2</sup>*CNRS, ENS de Lyon, Laboratoire de Physique (LPENSL UMR 5672), 69342 Lyon Cedex 07, France*

<sup>3</sup>*ENS de Lyon, Centre Blaise Pascal (CBPsmn), 69342 Lyon Cedex 07, France*

<sup>4</sup>*ENS de Lyon, CNRS, Laboratoire de Physique (LPENSL UMR 5672), 69342 Lyon Cedex 07, France*

The statistics of randomly branching double-folded ring polymers are relevant to the secondary structure of RNA, the large-scale branching of plectonemic DNA (and thus bacterial chromosomes), the conformations of single-ring polymers migrating through an array of obstacles, as well as to the conformational statistics of eukaryotic chromosomes and melts of crumpled, non-concatenated ring polymers. Double-folded rings fall into different dynamical universality classes depending on whether the random tree-like graphs underlying the double-folding are quenched or annealed, and whether the trees can undergo unhindered Brownian motion in their spatial embedding. Locally, one can distinguish (i) repton-like mass transport around a fixed tree, (ii) the spontaneous creation and deletion of side branches, and (iii) displacements of tree node, where complementary ring segments diffuse together in space. Here we employ dynamic Monte Carlo simulations of a suitable elastic lattice polymer model of double-folded, randomly branching ring polymers to explore the mesoscopic dynamics that emerge from different combinations of the above local modes in three different systems: ideal non-interacting rings, self-avoiding rings, and rings in the melt state. We observe the expected scaling regimes for ring reptation, the dynamics of double-folded rings in an array of obstacles, and Rouse-like tree dynamics as limiting cases. Of particular interest, the monomer mean-square displacements of  $g_1 \sim t^{0.4}$  observed for crumpled rings with  $\nu = 1/3$  are similar to the subdiffusive regime observed in bacterial chromosomes. In our analysis, we focus on the question to which extent contributions of different local dynamical modes to the emergent dynamics are simply additive. Notably, we reveal a non-trivial acceleration of the dynamics of interacting rings, when all three types of local motion are present. In the melt case, the asymptotic ring center-of-mass diffusion is dominated by the contribution arising from coupling of the ring-in-an-array-of-obstacles dynamics with the tree dynamics. This contribution scales inversely with the ring weight and is compatible with a scenario in which constraint release restores a Rouse-like dynamics.

## I. INTRODUCTION

Large ring polymers exhibit surprisingly rich behavior. When diffusing through an array of obstacles, they naturally adopt double-folded conformations, forming randomly branching polymer structures or trees [1–6] (Fig. 1). Interestingly, double-folded tree-like ring conformations have broad significance in biological systems. Examples include plectonemes in supercoiled DNA molecules [7–9] and, consequently, their role in bacterial chromosome structuring [8, 10–12], large RNA molecules [13–15], and the arrangement of DNA in eukaryotic cells during interphase, which bears striking similarities to the behavior of melts of non-concatenated ring polymers [16–18].

Double-folded rings fall into different dynamical universality classes depending on whether the random tree-like graphs underlying the double-folding are quenched or annealed [19], and whether the trees can undergo unhindered Brownian motion in their spatial embedding. Specifically, one can identify three distinct types of local

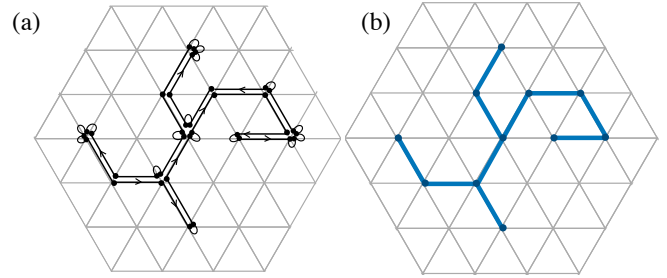


FIG. 1. (a) An example of a (tightly wrapped) double-folded ring polymer and (b) the corresponding tree on a trigonal lattice. Small loops represent reptons (bonds of zero length, see Section III), for which adjacent monomers along the ring occupy identical lattice sites.

dynamics:

1. **Reptons** transporting ring mass along a fixed tree [9, 20].
2. **Creation or retraction of side-branches** where either (i) one of the two double-folded ring segments double-folds onto itself and branches away from the current tree or where (ii) the ring seg-

\* ralf.everaers@ens-lyon.fr

ments wrapping a side branch are retracted into the rest of the tree in the inverse process.

### 3. Brownian motion of tree nodes

maintaining the tree connectivity and the secondary structure of the double-folded rings [21].

The effect of repeated local modifications (or “moves” in the Monte Carlo (MC) language we will adopt throughout the article) is not simply additive to the resulting dynamics of the ring and tree conformations. Instead, an *emergent dynamics* typically arises because the ring “monomers” and tree “nodes” are not independent degrees of freedom but are coupled through (i) the ring connectivity, (ii) the constraint of double-folding restricting ring conformations to those with underlying tree structures, (iii) additional Hamiltonian terms governing interactions between monomers or nodes, branching activity, or chain stiffness, and (iv) local topological constraints arising from the mutual impenetrability of ring and tree backbones.

This coupling is not a particularity of rings. In linear chains, the connectivity between successive monomers gives rise to the characteristic Rouse intrachain dynamics, while topological constraints are at the origin of the reptation dynamics in the tube model [22]. Dynamical analogues can be formulated for rings. In particular, a well-understood limit is the “ring-in-an-array-of-obstacles” (RiAO) dynamics [2, 6, 23], which arises from the coupling of local mass transport along the tree and the creation and deletion of side branches. However, understanding the general case remains a challenge, more particularly in the melt case, where the “obstacles” represent co-localized ring segments that are not fixed in space but instead have dynamics of their own [23]. The purpose of the present paper is to pave the way for solving this challenge by introducing:

- a model system, where the various interactions and types of local dynamics can be switched on and off in a controlled manner,
- a procedure to analyze the independency of contributions from different dynamic modes to the experimentally observable monomer and center-of-mass mean-square displacements.

The manuscript is structured as follows: In Section II we introduce the relevant observables and associated exponents, along with a brief summary of the theoretical background. In Section III, we introduce our model and the corresponding dynamic MC scheme to investigate its dynamical properties. In particular, this scheme extends our previous elastic lattice model for simulating tightly double-folded ring polymers, where only single monomers could move [24], by incorporating an additional tree node move akin to diffusive dynamics. We then explain how to systematically and in a fully controlled manner combine the different types of monomer and tree node

moves. Finally, we introduce the systems studied: ideal non-interacting double-folded rings, isolated self-avoiding double-folded rings, and melts of double-folded rings. In the Results Section IV, we briefly examine the well-understood static ring properties of these systems, which also serves to validate that the ensembles generated by different combinations of local dynamics remain identical as long as the system conditions are unchanged. We then focus on comparing the diffusion properties of both monomers and the center of mass across different dynamical schemes and available theoretical results. Notably, in melts, we find that the mixture of tree node and ring monomer moves leads to a non-trivial acceleration of the emergent dynamics. The subsequent Discussion Section V explores the functional form and amplitude of the dynamics arising from the coupling in a context that deals more generally with the analysis of data from mixed dynamical schemes and the question of how to identify and distinguish non-trivial coupling effects from situations where the contributions of different local modes to the emergent dynamics are independent. Finally, we provide a brief conclusion in Section VI.

## II. THEORETICAL BACKGROUND

### A. Static Properties

The behavior of a double-folded ring polymer [1–3, 5, 6, 25, 26] can be analyzed through three structural levels [21] (Fig. 1). The primary structure is defined through the connectivity of the monomers along the ring. The secondary structure corresponds to the double folding. It can be represented by mapping the ring onto a graph with the connectivity of the tree. The tertiary structure is defined by the positions of the ring monomers and tree nodes within the embedding (three-dimensional) space. A small set of exponents describes how the expectation values of typical observables scale with the ring weight  $N$  (the number of monomers):

$$\langle L(N) \rangle \sim N^\rho, \quad (1)$$

$$\langle R_g^2(N) \rangle \sim N^{2\nu}. \quad (2)$$

where  $L$  is the mean tree contour distance (the shortest distance on the tree) between tree nodes,  $R_g$  is the radius of gyration of the ring [24]. For ideal, non-interacting systems, the exponents are  $\rho = 1/2$  and  $\nu = 1/4$  [27, 28]. For interacting systems, the only known exact result is the value  $\nu = 1/2$  for self-avoiding trees in  $d = 3$  [29]. Otherwise, Flory theory [4, 19, 30–32] predicts  $\rho = 2/3$  for self-avoiding trees, and  $\nu = 1/3$  and  $\rho = 5/9$  for trees in the melt state.

## B. Dynamical Properties

A typical analysis of polymer dynamics involves monitoring, as a function of time:

- the total monomer mean-square displacement (MSD)

$$g_1(t) = \langle |\mathbf{r}_i(t) - \mathbf{r}_i(0)|^2 \rangle \quad (3)$$

- the monomer MSD relative to the chain's center of mass (CM)

$$g_2(t) = \langle |\mathbf{r}_i(t) - \mathbf{r}_{CM}(t) + \mathbf{r}_{CM}(0) - \mathbf{r}_i(0)|^2 \rangle \quad (4)$$

- the MSD of CM

$$g_3(t) = \langle |\mathbf{r}_{CM}(t) - \mathbf{r}_{CM}(0)|^2 \rangle. \quad (5)$$

On time scales where the rings have moved beyond their own size, their CM exhibit diffusive motion:  $g_1(t) = g_3(t) \sim t$ , and  $g_2(t) = 2\langle R_g^2 \rangle$ . On shorter time scales, the internal dynamics can display a range of intermediate scaling regimes, whose understanding is important to comprehend the diffusion constant in the asymptotic regime. A summary of the scaling exponents for  $g_1(t)$ ,  $g_3(t)$ , and the diffusion constant  $D$  in the known limiting cases discussed below are given in Table I.

### 1. Slithering dynamics of tightly wrapped rings around fixed trees

For local mass transport via reptons along a fixed tree [9, 20, 22, 33, 34], the monomer motion *in the embedding space* is given by:

$$g_1(t) \sim \langle \delta s^2(t) \rangle^\nu. \quad (6)$$

where  $\langle \delta s^2(t) \rangle$  denotes the one-dimensional monomer MSD *along the tree*. Several regimes must then be distinguished. First, for the shortest time scales,  $\langle \delta s^2(t) \rangle \sim t$ , so that:

$$g_1(t) \sim t^\nu. \quad (7)$$

At longer time scales, the ring connectivity gives rise to a one-dimensional Rouse dynamics typical of a linear polymer,  $\langle \delta s^2(t) \rangle \sim t^{1/2}$ , so that:

$$g_1(t) \sim t^{\frac{\nu}{2}}. \quad (8)$$

Beyond the Rouse time,  $\tau_R \sim N^2$  where  $g_1(\tau_R) \sim N^\nu \sim \sqrt{\langle R_g^2 \rangle}$ , the dynamics crosses over to the reptation regime where all monomers diffuse coherently around the tree. Again  $\langle \delta s^2(t) \rangle \sim t$ , so that:

TABLE I. Summary of the scaling exponents for  $g_1$ ,  $g_3$ , and  $D$  for ideal rings, isolated self-avoiding (S.A.) rings, and rings in the melt state.

	$g_1$	$g_3$	$D$
Ideal rings			
Rouse Dynamics for the quenched tree	1/3	1	-1
Ring in an array of obstacles	1/5	3/5	-2
Ring slithering around the tree	1/4, 1/8, 1/4	1/2	0
S.A. rings			
Rouse Dynamics for the quenched tree	1/2	1	-1
Ring in an array of obstacles	3/8	3/4	-5/3
Ring slithering around the tree	1/2, 1/4, 1/2	1/2	0
Melt rings			
Rouse Dynamics for the quenched tree	2/5	1	-1
Ring in an array of obstacles	6/23	15/23	-17/9
Ring slithering around the tree	1/3, 1/6, 1/3	1/2	0
FLG	2/7	5/7	-5/3

$$g_1(t) \sim t^\nu, \quad (9)$$

but, compared to the shortest time scales, with a  $N$  times smaller diffusion constant of the one-dimensional CM motion. Finally, as the ring diffuses along a fixed, closed path, the monomer displacements reach a plateau at  $2\langle R_g^2 \rangle$ .  $g_3(t) \ll \langle R_g^2 \rangle$ , because fluctuations in the ring CM are only due to negligible density fluctuations along a ring, which is stretched over a path whose length is of the order of the ring length.

### 2. Rings in an array of fixed obstacles

The combination of repton moves with the local creation or retraction of side branches gives rise to the characteristic motion of rings in an array of fixed obstacles [2, 6] suppressing the sideways motion of tree nodes. Specifically,  $g_1(t) \sim t^{\frac{2\nu}{2+\rho}}$  and  $g_3(t) \sim t^{\frac{2\nu+1}{2+\rho}}$  in the intermediate regime. Moreover, the CM diffusion coefficient is found to scale as  $D \sim N^{-2-\rho+2\nu}$  [6].

### 3. Brownian dynamics of randomly quenched trees

The emerging dynamics of quenched trees, where only tree nodes can diffuse via Brownian motion, are expected to be described by a suitably generalized Rouse model [35] predicting free diffusion of the tree CM at all time scales,  $g_3(t) \sim t/N$ ,  $g_1(t) \sim t^{\frac{2\nu}{2\nu+1}}$  in the intermediate regime and  $g_1(t) \sim t$  on the shortest time

scales. Moreover, the CM diffusion coefficient is expected to scale as  $D \sim N^{-1}$ .

#### 4. Rings in an array of transient obstacles

The dynamics in the melt state is subject to local topological constraints due to the mutual impenetrability of double-folded ring sections. However, to the extent that the rings move, these constraints are not fixed, but transient. The recent *fractal loopy globule* (FLG) model, incorporates the effect of moving obstacles on the dynamics of the target ring [36]. According to this model, topological constraints in the melt state gradually dilute over time. This occurs because, as time progresses, larger loops relax, eventually no longer acting as obstacles. This process is analogous to the tube dilation phenomenon observed in polydisperse linear melts [37–39]. The FLG model predicts the scaling of the mean square displacement as  $g_1(t) \sim t^{\frac{2\nu}{2+\nu}}$ , and diffusion coefficient scaling as  $D \sim N^{-2+\nu}$ .

### III. MODEL AND METHOD

#### A. Discrete Double-Folded Ring Model

We consider discrete rings made of  $N_m$  monomers and embedded in a face-centered cubic (FCC) lattice, with the mesh size (i.e., the space unit) set to 1. Following previous works [3, 24] and the original elastic lattice polymer models [40–43], we include the possibility that two successive monomers along the ring may occupy the same lattice site. In this case, the bond length between these monomers is 0 (referred to as the stored length), compared to 1 for extended bonds (Fig. 1a). The double-folded nature of the model is then imposed by pairing each extended bond of the double-folded polymer with an opposing extended bond, as shown in Fig. 1a.

#### B. Handling the Underlying Lattice Tree

A randomly double-folded ring polymer is characterized by an underlying randomly branched tree structure [1–3, 5, 6, 25, 26]. This tree is an undirected graph, whose nodes (vertices of the graph) are located on the occupied lattice sites and edges correspond to double-folded ring bonds. By definition, the tree is acyclic, and any pair of tree nodes is connected through a unique shortest path on the tree. Fig. 1 provides a visual 2D representation of a double-folded ring together with its underlying tree structure.

In our previous work [24], we simulated double-folded ring polymers and characterized the corresponding tree

conformations only during post-processing. This is unproblematic in systems with hard excluded volume interactions, where a ring configuration corresponds to a unique tree structure, because all spatially co-localized monomers belong to the same tree node (Fig. 1). However, in ideal double-folded rings, multiple tree nodes may occupy the same lattice site, introducing ambiguity in defining the underlying tree structure [24] and the statistical weight of ring conformations [44]

To solve this problem, we extend the description of the double-folded ring by considering the degrees of freedom associated with the underlying tree. To this end, we define a ring conformation ( $\mathcal{C}$ ) by its set of  $(N_m)$  monomer positions in the embedding space,  $\{\vec{r}_1, \vec{r}_2, \dots, \vec{r}_{N_m}\}$  together with its set of  $(N_n)$  tree node positions,  $\{\vec{R}_1, \vec{R}_2, \dots, \vec{R}_{N_n}\}$ , the ring and tree connectivity graphs, and information about which monomers belong to which tree node. For ideal systems we impose the constraint that nearest-neighbor tree nodes must not overlap, i.e.  $|\vec{R}_I - \vec{R}_J| = 1$ , which is automatically fulfilled in systems with hard excluded volume interactions. As a consequence, there are small differences in the local structure of the present ideal rings and those of [24]. A summary of the data structure is presented in Table II.

In this context, the functionality  $f$  of a tree node (the degree of a vertex) is defined by the number of tree edges coming out from the node. Specifically, a node with  $f = 1$  corresponds to a leaf or branch tip,  $f = 2$  to a linear section of the double-folded ring, and  $f \geq 2$  to a branching point. For simplicity, and without loss of generality [5], here we limit the functionality to  $f_{\max} = 3$ .

#### C. Dynamic Monte Carlo Scheme for Mixed Dynamics

To investigate the dynamical properties of double-folded rings, we performed dynamic MC simulations. To this end, we used two types of monomer moves and one

	Ring Monomer $i$	Tree Node $I$
Position	$\vec{r}_i$	$\vec{R}_I$
Functionality	2	$f_I$
Connectivity	$\Gamma(i) = \{i-1, i+1\}$ $ \Gamma(i)  = 2$	$\Gamma(I) = \{J, K, \dots\}$ $ \Gamma(I)  = f_I$
Bond Constraints	$ \vec{r}_i - \vec{r}_{i+1}  \in \{0, 1\}$	$ \vec{R}_I - \vec{R}_J  = 1 \quad \forall J \in \Gamma(I)$
Ring $\leftrightarrow$ Tree	$i \rightarrow I$	$I \rightarrow \{i, j, k, \dots\}$

TABLE II. Data structure defining the conformation ( $\mathcal{C}$ ) of a double folded ring polymer and the associated tightly wrapped tree.

new type of tree node move (see first subsection below), together capturing the three possible types of local dynamics in double-folded polymers: reptons, creation/retraction of side branches, and Brownian motion of tree nodes. In addition, when considering volume exclusion (see systems studied in Section III E), we employed a Metropolis algorithm, setting a very high interaction energy (i.e., greater than 30 units of thermal energy) between nodes on the same lattice site, with no interaction otherwise.

As explained in the second subsection below, we then combined these three types of trial moves to generate mixed dynamics in a controlled manner, ensuring that the time unit reflects the fraction of time each type of move is selected.

### 1. Trial moves

Trial moves consist of individual monomers or tree nodes attempting to hop to adjacent lattice sites, with three distinct types:

**Repton (monomer) move:** This occurs when a monomer hops longitudinally along the ring, crossing an extended bond to a neighboring tree node, thereby transporting a unit of stored length along the tree without changing its structure or the system's energy. An example is shown in Fig. 2a.

**Hairpin (monomer) move:** This occurs when a monomer flanked by two zero-length bonds hops in a transverse direction, extending or creating a side branch. During the move, both zero-length bonds unfold, generating two new paired, oppositely oriented extended bonds. Consequently, the moved monomer is reassigned to a new node of functionality  $f = 1$ . This new node connects to the node to which the monomer was originally associated, increasing the latter's functionality by one, as well as the total number of tree nodes,  $N_n - N_n$  thus varies during a simulation involving hairpin moves. The corresponding inverse move removes an extended bond pair, leading to the shortening or complete removal (annihilation) of a side branch. An example is shown in Fig. 2b.

**Tree node move:** This occurs when a tree node moves with all its associated monomers without changing the length of any of the involved tree edges and ring bonds. These moves thus preserve the tree structure and the association between the tree and the ring. Examples are shown in Fig. 2c-d.

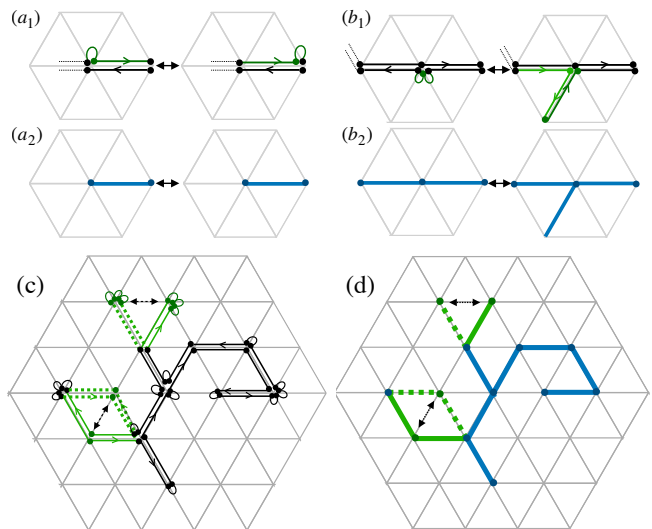


FIG. 2. (a)-(b): One monomer move involves hopping a randomly selected monomer into the nearest neighbor lattice site. (a) The Repton move; is responsible for the local redistribution of stored lengths. (b) The Hairpin move; is responsible for the creation or annihilation of side branches. The top row shows the double-folded ring, and the bottom row shows the underlying tree structure. (c)-(d) Two examples of tree node trial moves attempting to displace a randomly selected tree node to a randomly chosen site out of twelve possible nearest neighbors under a double-folding preserving constraint.

### D. Mixed Dynamics and the Unit of Time

In dynamic MC simulations, the (effective) time unit  $\tau$  is equivalent to one MC sweep comprising a number of  $M_s$  MC trials or steps chosen such that each component of the system is selected on average once. For instance, if the dynamics consists solely of repton or hairpin moves, a sweep comprises  $M_s = N_m$  trials, associating a duration of  $\tau_m = \tau/N_m$  with an individual MC step. If the dynamics consists solely of tree node moves, a sweep instead consists of  $M_s = N_n$  trials and the time associated with a step is  $\tau_n = \tau/N_n$ . In particular,  $\tau_n/\tau_m = N_m/N_n > 1$  because a node move displaces several associated monomers.

A natural way to define a mixed dynamics is to randomly alternate monomer and tree node *sweeps* with probabilities  $p_m \in [0, 1]$  and  $(1 - p_m)$  respectively. For  $p_m = 1$  this essentially generates the rings-in-an-array-of-obstacles dynamics from Ref. [24], while  $p_m = 0$  simulates the Brownian dynamics of quenched trees. Intermediate values mix the two types of motion in arbitrary proportions.

In the above scheme a total of  $t$  sweeps corresponds to  $p_m N_m t$  monomer moves and  $(1 - p_m) N_n t$  node moves. In practice, we have used the following scheme to alternate between monomer and node *steps* in such a way as to preserve the above proportions:

1. Compute the number  $M_s$  of MC steps for the next sweep as:

$$M_s = p_m N_m + (1 - p_m) N_n \quad (10)$$

Note that since  $N_n$  can vary,  $M_s$  can also vary, but that irrespective of the value of  $N_n$  moving all tree nodes always corresponds to moving all monomers.

2. Perform  $M_s$  trials, selecting a monomer move with probability  $p_m N_m / M_s$  and a tree node move with probability  $(1 - p_m) N_n / M_s$ .
3. Increment time by 1.

By construction,  $p_m N_m \tau_m + (1 - p_m) N_n \tau_n = \tau$  and a monomer is moved on average once per sweep.

In addition, we have introduced acceptance probabilities  $0 \leq q_{rep}, q_{hp} \leq 1$  for the two monomer moves. For  $q_{rep} = 0$  and  $q_{hp} = 1$ , all Repton moves are suppressed, resulting in dynamics that involve only the Hairpin moves. In the opposite case of  $q_{rep} = 1$  and  $q_{hp} = 0$ , the only accepted monomer moves are Repton moves generating mass transport along the tree. While equal values  $0 \leq q_{rep} = q_{hp} < 1$  generate a slowed down version of the original dynamics, other choices allow to arbitrarily manipulate the relative weight of Repton and Hairpin moves.

### E. Systems Studied and Equilibrium Preparation

We performed simulations for double-folded rings composed of  $N_m = 64, 125, 216, 343, 512, 1000$  monomers on a three-dimensional FCC lattice with periodic boundary conditions for three types of systems: ideal rings, isolated self-avoiding rings, and rings in the melt state. For the ideal rings, there were no restrictions on the number of tree nodes per lattice site (i.e., no excluded volume interaction). For the self-avoiding rings and the rings in the melt state, we included excluded volume interactions (explained in Section III C). Self-avoiding rings were simulated in a sufficiently large box, while a high lattice occupation number,  $\phi \simeq 0.93$ , was used for the melt state. A summary of the simulation parameters and equilibrium values for the studied systems is provided in Table I in Supplementary Material.

All reported results were generated by first fully equilibrating the system according to the protocol of [24], using monomer moves for annealed double-folding rings (see Supplementary Material, Section I). Then, at the initial time of all simulation runs, an “equilibrated” state was randomly chosen.

## IV. RESULTS

To set the stage, we begin with a brief overview of the systems’ static properties in Section IV A, which

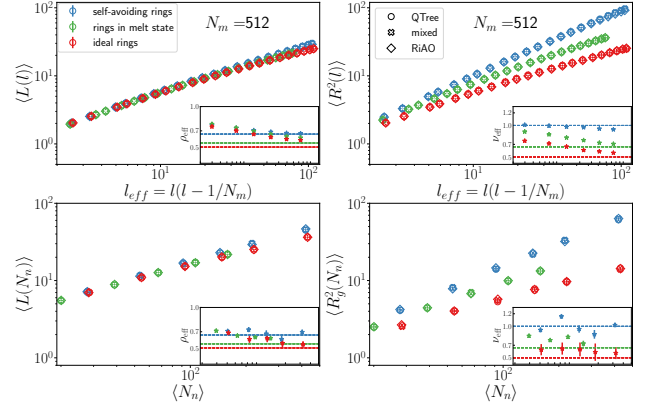


FIG. 3. Conformational statistics for isolated ideal rings, isolated self-avoiding rings, and rings in the melt state when subjected to Quenched Tree dynamics (QTree), ring in an array of obstacle-like (RiAO) dynamics, and the combination of the two (mixed). Inset panels show the local slopes of the data and the horizontal dashed lines correspond to the expectation scaling exponents for each system. The conformational statistics should be independent of the dynamics if the system condition remains the same and the results in the figure strongly confirm this assertion. Error bars are the same size or smaller than the symbols.

also serves to validate our simulation methods. In Sections IV B and IV C, we analyze the emergent dynamics of monomers and CM for different combinations of trial moves.

### A. Static Properties

In Figure 3 we present a number of results characterizing the secondary structure and the tertiary structure of our double folded rings along the lines of Ref. [21, 24]. Different colors distinguish results for ideal, self-avoiding and melt systems, while the symbols indicate the type of dynamics we used to acquire the data.

Specifically we have calculated for all pairs  $(i, j)$  of ring monomers their distance,  $L(i, j)$ , on the graph and their square distance,  $R^2(i, j)$ , in space. Averages as a function of the ring contour distance,  $l = |i - j| \langle b \rangle$  are plotted in the top row of Fig. 3. The average bond length  $\langle b \rangle$  is smaller than one, since the monomer bonds can be 0 or 1 due to the presence of reptons in our model. Note that the data shown in the top row of Figure 3 is plotted as a function of the effective ring contour distance,  $l_{eff} = l(1 - 1/N_m)$ , as a means of reducing finite ring size effects [21]. As a complement, we averaged  $L(i, j)$  and  $R^2(i, j)$  over all monomer pairs of our rings to calculate the average tree contour distance  $\langle L \rangle$  and the mean-square gyration radius  $\langle R_g^2 \rangle$ . Results as a function of the average number of tree nodes,  $\langle N_n \rangle$ , are plotted in the panels in the bottom row of Fig. 3. A summary of these

values for the studied systems is provided in Table I in the Supplementary Material. Additionally, we calculated the effective local exponents,  $\rho_{eff}$  and  $\nu_{eff}$ , from the slopes of the data points shown in the four panels of Fig. 3. The results are presented in the insets of the corresponding panels.

In absolute terms, the differences between the average tree contour distances,  $\langle L(l_{eff}) \rangle$  and  $\langle L(N_n) \rangle$ , for the three ring types are small. Nevertheless our data are compatible with the expected crossover from local linear behavior with  $\langle L(l) \rangle = l$  to  $\langle L(l) \rangle \sim l^\rho$  with  $\rho = 1/2$  for ideal trees,  $\rho = 2/3$  for self-avoiding trees, and  $\rho = 5/9$  for trees in the melt state.

In contrast, there are marked differences between the mean square spatial distance between ring monomers,  $\langle R^2(l_{eff}) \rangle$  and  $\langle R^2(N_n) \rangle$ , for the different ring types. For ideal trees, this quantity is given by [45]  $\langle R^2(l) \rangle = l_K \langle L(l) \rangle$ , where the Kuhn length  $l_K$  for the present model is simply given by the lattice constant. The fact that the independently calculated data sets for  $\langle L(l_{eff}) \rangle$  and  $\langle R^2(l_{eff}) \rangle$  look indistinguishable presents a simple and independent check of the path analysis on the tree. As expected, self-avoiding rings are more strongly swollen relative to ideal rings than rings in a melt. Again, our data are compatible with the expected crossover from local linear behavior with  $\langle R^2(l) \rangle = l$  to  $\langle R^2(l) \rangle \sim l^{2\nu}$  with  $\nu = 1/4$  for ideal trees,  $\nu = 1/2$  for self-avoiding trees, and  $\nu = 1/3$  for trees in the melt state. Note, however, the deviation of the effective exponents on small scales from the expected asymptotic values, which suggests the existence of corresponding deviations for effective dynamic exponents.

Importantly, for our present purposes, there are no noticeable differences between the data acquired through different dynamical schemes. Figure 3 thus validates our simulation methods and confirms that starting from an ensemble of equilibrated rings all ergodic dynamical schemes generate the same conformational statistics independently of whether the tree connectivity is randomly quenched or annealed.

## B. Overview of the Emergent Dynamics

Figure 4 presents an overview of the emergent dynamics for three classes of double-folded rings – ideal rings (top row), isolated self-avoiding rings (middle row), and ring polymers in melts (bottom row) – for which we have investigated the impact of the following local dynamics:

1. the exclusive application of hairpin moves,
2. a slithering dynamics around fixed trees as a result of the exclusive application of repton moves,
3. a RiAO dynamics as a result of the combined application of the two monomer moves,

4. a Brownian dynamics of trees with quenched connectivity (QTree) as a result of the exclusive application of tree node moves,
5. the combination of ring monomer and tree node moves, using  $p_m = 0.5$ .

Results for the monomer MSD,  $g_1(t)$ , the CM MSD,  $g_3(t)$ , and the size dependence of the asymptotic CM diffusion constants  $D = \lim_{t \rightarrow \infty} \frac{g_3(t)}{6t}$ , are presented in separate panels in the three columns of the figure. In addition, we report results obtained for the combination of repton and tree node moves in Fig. 9 in Appendix B.

While hairpin moves can locally redistribute accumulations of stored length, the overall dynamics emerging from their exclusive application is close to negligible: the final plateau is reached after approximately  $\sim 30M_s$ , with monomer and CM MSDs remaining strictly proportional to each other, i.e.,  $g_1(t) = N_m g_3(t)$ . In contrast, the slithering dynamics emerging from the exclusive application of repton moves allows ring monomers to explore, in the long run, all sections of a wrapped, fixed tree. The confinement of the motion becomes visible notably earlier for the ring's CM than for individual monomers. Importantly, it is only the combination of the two monomer moves that renders the RiAO dynamics ergodic. Interestingly, the absolute magnitude of the latter varies only weakly between the three considered systems.

For ideal and isolated self-avoiding rings, the quenched tree (QTree) dynamics is significantly faster than the RiAO dynamics, because in the intermediate scaling regime the exponents describing the (in general anomalous) monomer and CM diffusion are effectively larger. As a consequence, the rings equilibrate more quickly as it takes them less time to displace over distances comparable to their own size.

The situation is quite different in the melt case, where the hard-excluded volume interactions and the high occupation number ( $\phi \sim 0.93$ ) of the lattice cells induce a strong reduction in the acceptance probability of hairpin and tree node moves. The early-time monomer dynamics, in particular, is now significantly slower for QTree dynamics than for RiAO dynamics. However, the anomalous diffusion in the intermediate regime appears to be faster for the QTree dynamics. Our data for the size dependence of the diffusion constant,  $D(N_n)$ , (bottom right panel in Fig. 4) suggest that the Brownian QTree dynamics is, at least for the present melts, asymptotically faster than the RiAO dynamics.

For ideal and isolated self-avoiding rings, the MSD resulting from the combination of ring monomer and tree node moves is unremarkable, displaying an intermediate behavior between the MSD emerging from the exclusive application of either monomer moves or node moves. Namely, with our definition of a MC sweep as the unit of time (see Section IIID), the mixing of 50% tree node moves and 50% of the much less effective monomer moves essentially slows down the motion by a factor of two in



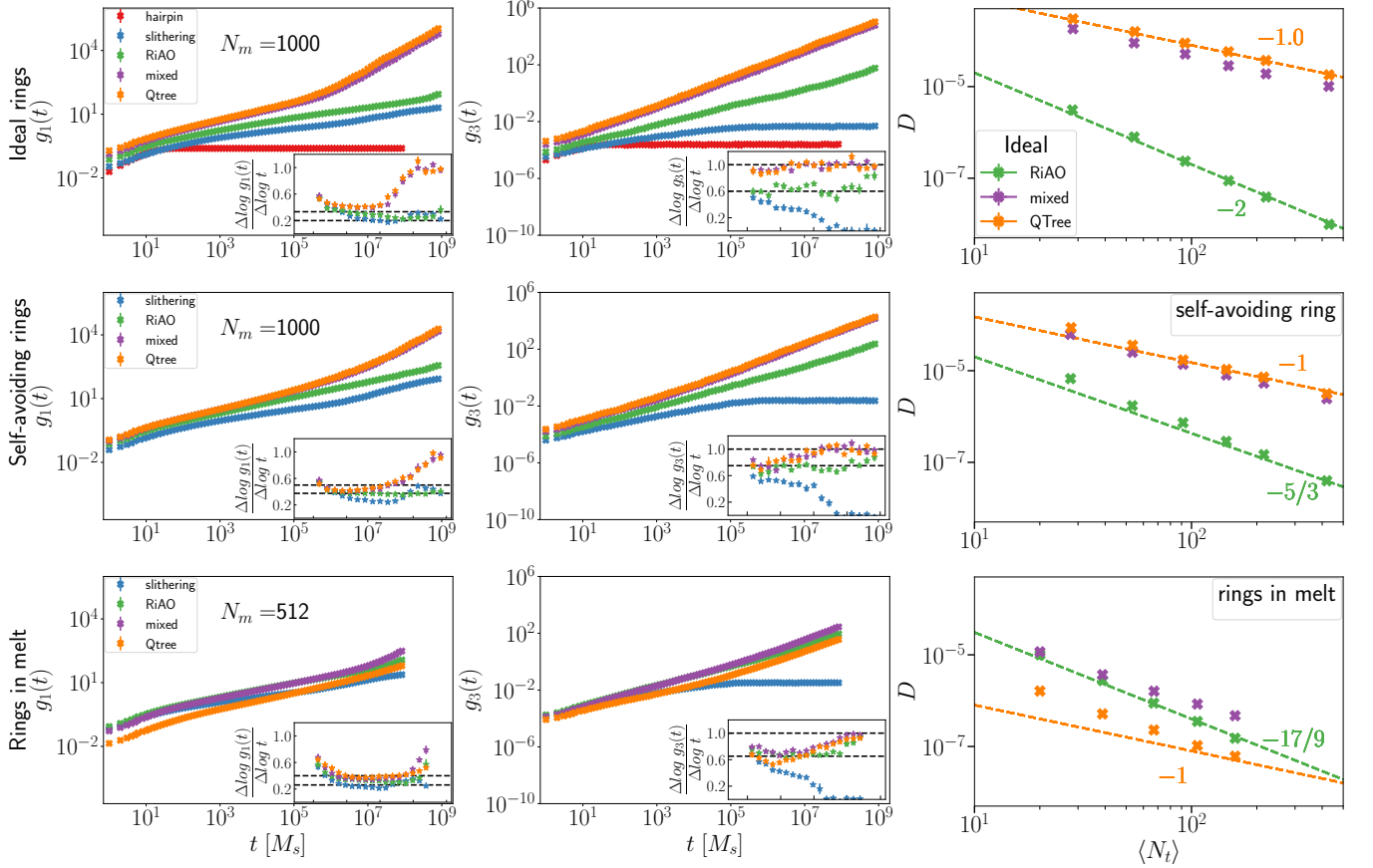


FIG. 4. Overview of emergent dynamics for different ring polymer systems: ideal (top row), isolated self-avoiding (middle row), and double-folded ring polymers in melts (bottom row). Results are shown for: monomer MSD,  $g_1(t)$  (left column), CM MSD,  $g_3(t)$ , (middle column) and the size dependence of the asymptotic CM diffusion constants,  $D(N_n)$ , (right column). Dynamics considered include: hairpin move, slithering dynamics, ring-in-an-array-of-obstacles (RiAO)-like dynamics, quenched tree dynamics (QTree), and a mix of RiAO and QTree dynamics. Insets show the local slopes of the data, with dashed lines indicating the expected exponents for QTree and RiAO dynamics (summarized in Table I). Error bars are smaller than or comparable to the symbol sizes.

time. By contrast, and notably, something interesting happens in the melt case: *the mixed dynamics is faster than either of the pure components*, what we investigate in detail below.

### C. Scaling analysis of the Emergent Dynamics

Before analyzing in detail the speed-up associated with the combined dynamics, we first present a detailed scaling analysis of the dynamics reported in Fig. 4. This analysis begins with the three limiting cases discussed in the Theoretical Background (Section II) and concludes with the mixed dynamics.

Specifically, in Fig. 5 we report scaling results for  $g_1$  and  $g_3$  in the context of the exclusive application of repton moves (slithering dynamics), for ideal trees. In Fig. 6, we report corresponding scaling results in the context of three other dynamics – the RiAO dynamics (left col-

umn), the Brownian motion of trees (central column) and the combined dynamics (right column) – for ideal rings (top row), self-avoiding rings (middle row), and rings in melts (bottom row). Additional details and figures can be found in Section II of the Supplementary Material.

#### 1. Slithering dynamics around fixed ideal trees

Let us first consider the slithering dynamics around a fixed (quenched) tree emerging from the exclusive application of repton moves. In Fig. 5 in the Supplementary Material, we show the corresponding monomer and CM MSD for ideal randomly branching double-folded rings composed of  $N_m = 64, 216, 512, 1000$  monomers. An obvious feature is the nearly absent CM motion of the rings,  $g_3(t) < \langle R_g^2(N_m) \rangle / N_m$ , such that  $g_1(t) \approx g_2(t)$ . We then use various rescaling of the same data in the different panels of the figure to reveal different time



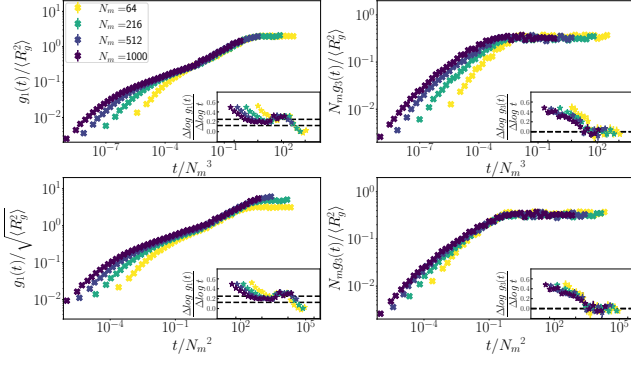


FIG. 5. Scaling analysis of the slithering dynamics of ideal randomly branching double-folded rings emerging from the exclusive application of repton moves in our model.

and length scales relevant to the monomer and the CM motion. Namely, the ring monomers are fully mobile while remaining bound to the quenched tree conformations that the rings are wrapping. As a consequence,  $\lim_{t \rightarrow \infty} g_2(t) = 2\langle R_g^2(N_m) \rangle$ . The asymptotic plateau is reached on the reptation time scale,  $\tau_{rep} \sim N_m^3$ , of the *rings*, while the crossover from the  $t^{\nu/2}$  to the  $t^\nu$  regime in monomer diffusion occurs at their Rouse time,  $\tau_R \sim N_m^2$ .

The CM of the rings essentially coincide with the CM of their wrapped tree. The observable small deviations are due to monomer density fluctuations along the ring contour and equilibrate over the Rouse time,  $\tau_R \sim N_m^2$ , of the *rings*. The asymptotic magnitude of the fluctuations are expected to be  $g_3(t \gg \tau_R) = 2 \frac{N_{rep}}{N_m^2} \langle R_g^2 \rangle$ .

## 2. RiAO-like dynamics

As already discussed in detail in Ref. [24], the emerging dynamics resulting from a combination of repton and hairpin moves agrees with the theoretical predictions for the RiAO model (Refs. [2, 6] and Sec. II). As shown in the left column of Fig. 6, an appropriate rescaling of our present data leads again to good agreement with the predicted  $g_1(t) \sim t^{\frac{2\nu}{2+\rho}} t$  and  $g_3(t) \sim t^{\frac{2\nu+1}{2+\rho}}$  for the monomer and tree CM dynamics. The corresponding effective dynamic exponents are shown in the insets of the panels. At least qualitatively, their slow decay in the tree scaling regime agrees with what one would expect from estimating the dynamic exponents from the effective static exponents,  $\rho_{eff}$  and  $\nu_{eff}$ , shown in Fig. 3. As shown in the middle column of Fig. 4 (green crosses), there is also good agreement between the predicted and the observed ring weight dependence of the asymptotic CM diffusion constants.

## 3. Brownian dynamics of randomly quenched trees

The emerging dynamics resulting from the exclusive application of tree node moves to our double-folded rings is presented in the central column of Fig. 6.

For ideal and self-avoiding trees, our data are in good agreement with the predictions of the Rouse model (Table I). The ring CM essentially exhibits simple diffusion,  $g_3(t) \sim t/N_m$ , with a diffusion constant inversely proportional to the number of ring monomers. A slowdown occurs independently of the ring size only over the first 50 MC sweeps in the ideal trees, while in the self-avoiding case, the slowdown persists for a longer duration, up to 1000 sweeps.

The monomer dynamics,  $g_1(t)$ , in the intermediate intra-chain scaling regime also approaches the prediction  $g_1(t) \sim t^{\frac{2\nu}{2\nu+1}}$  of the Rouse model (Table I). Again, the slow decay of the effective exponents reported in the detailed analysis in Fig. 6 agrees, at least qualitatively, with the observed crossover of the static exponents in Fig. 3.

Interestingly, the observed monomer MSDs in the melt are also in reasonable accord with the prediction  $g_1(t) \sim t^{0.4}$  of the Rouse model. However, the ring CM clearly exhibits anomalous diffusion in the intermediate regime. Experimental studies on ring polymers in the melt state have reported a substantial slowdown in COM dynamics [46–48], which occurs before the system reaches the free diffusion regime.

## 4. Combining monomer and node moves

The emerging dynamics resulting from the combination of ring monomer and tree node moves in equal proportions ( $p_m = 0.5$  in Eq. 10) are presented in the right column of Fig. 6.

Given that the node dynamics is significantly faster than the monomer dynamics in ideal and isolated self-avoiding systems (see Fig. 4), it is unsurprising that the former dominates the combined dynamics entirely, causing the resulting scaling plots to essentially collapse onto those in the central column.

It is tempting to draw similar conclusions in the melt case, but with respect to the left column of Fig. 6 and a faster RiAO-like dynamics (bottom row in Fig. 4). Yet, the situation is more subtle since the overall dynamics is accelerated with respect to the pure dynamics of either monomer moves or tree node moves. The excellent scaling of the data reported in the bottom right panel of Fig. 6 is thus in itself an interesting observation. We have tentatively included slopes predicted by the FLG model, but it is difficult to draw any quantitative conclusions at this point.

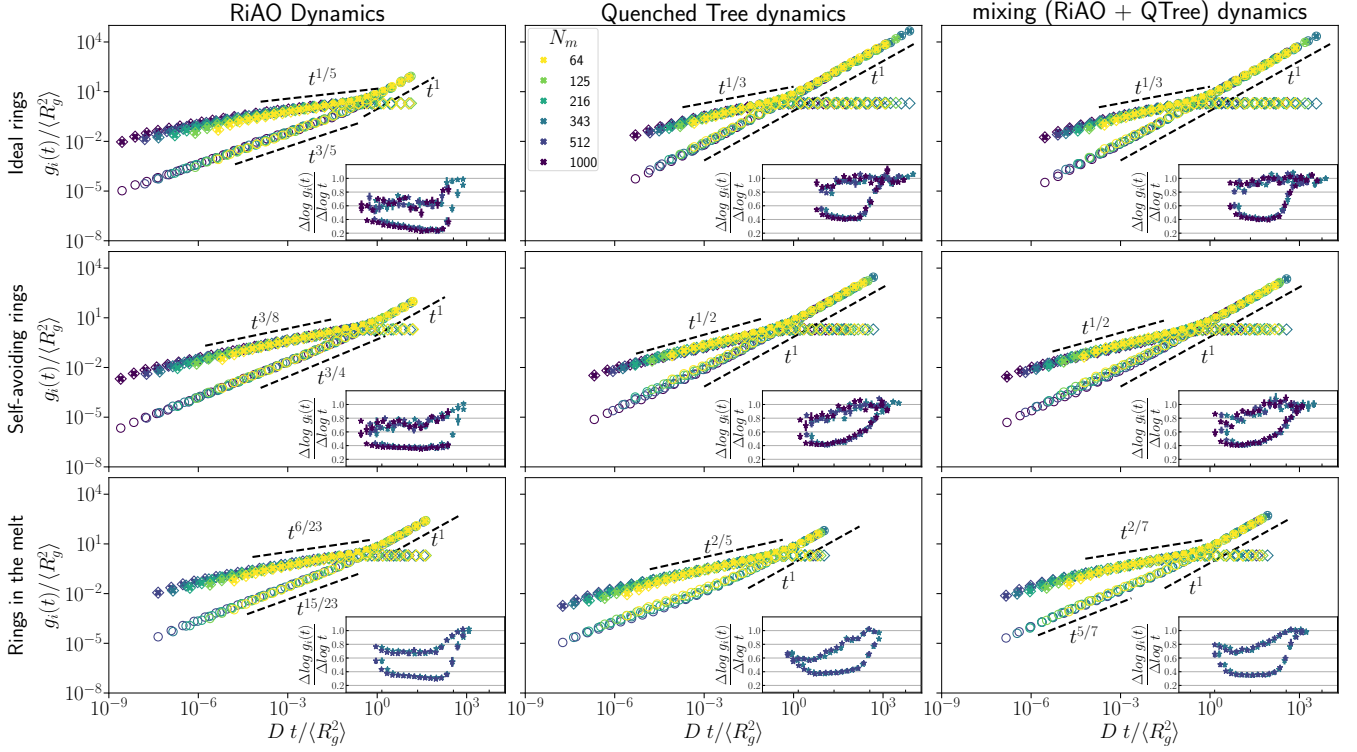


FIG. 6. Scaling behavior for  $g_1(t)$  (diamonds) and  $g_3(t)$  (circles) for three systems: ideal (top row), isolated self-avoiding (middle row), and double-folded ring polymers in melts (bottom row). Time is rescaled by the relaxation time, defined as  $\tau_{\max} = \frac{\langle R_g^2 \rangle}{D}$ . Left column: Results for RiAO-like dynamics. Middle column: Results for Brownian dynamics of randomly quenched trees. Right column: Results for a mixed of the two dynamics, with  $p_m = 0.5$  in Eq. 10.

## V. DISCUSSION

At this point, we have established a simulation scheme for double-folded ring polymers, which allows us to (i) simultaneously update and trace compatible ring and tree degrees of freedom and (ii) study the emerging dynamics resulting from the combination of different types of local dynamics. Our simulations in the context of ideal rings, self-avoiding rings and rings in melts accurately reproduce well-known dynamic properties of three prototypical systems: tightly wrapped rings slithering around fixed trees, rings in an array of obstacles and Brownian motion of trees with quenched connectivity.

The remaining challenge is to develop a protocol for the analysis of data obtained in mixed dynamical schemes. In particular, this protocol should allow us to identify and distinguish situations where the contributions of different local modes to the emergent dynamics are independent from those where the emergent dynamics arise from coupling effects.

To this end, let us consider two (asymptotically) diffusive processes,  $A$  and  $B$ , in a  $d$ -dimensional space, generating MSDs  $g_A(t) = 2dD_A t$  and  $g_B(t) = 2dD_B t$ , respectively. We are interested in the MSD  $g_{AB}(t)$  of

mixed schemes, where the local degrees of freedom are updated by  $A$  and  $B$  moves with probabilities  $p_A$  and  $p_B$ , respectively, and where typically (but not necessarily)  $p_A + p_B = 1$ . The null model of independent contributions from the  $A$  and  $B$  dynamics predicts an additive relationship for the resulting diffusion constant:

$$D_{AB}(p_A, p_B) = p_A D_A + p_B D_B \quad (11)$$

In Appendix A we propose, with Eq. (A4), an approximate plausible generalization of Eq. (11) for the full time dependence of the null model, for the monomer and CM MSDs in a mixed scheme. In Fig. 9 in Appendix B, we show that Eq. (A4) works well in a case where we expect the null model to apply: the dynamics emerging from the combination of repton and tree node moves, which are indeed completely decoupled within our model.

While the ergodic RiAO dynamics provides an interesting example of the emergence of a qualitatively different dynamics from the combination of local moves (see Appendix C), in the remainder of the (main) text, we focus on the emerging dynamics resulting from the combination of monomer and node moves in different proportions,  $0 \leq p_m \leq 1$ , see Eq. 10. As evident from Figs. 4 and 10, in interacting systems, this combination can lead to an accelerated dynamics compared to the two limiting

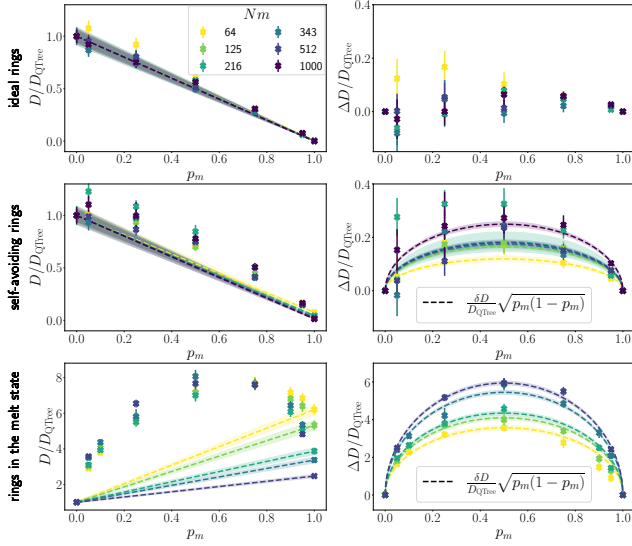


FIG. 7. Left column: The asymptotic center-of-mass (CM) diffusion constants for different systems, obtained using a combination of monomer and node moves in varying proportions ( $0 \leq p_m \leq 1$ ), as described in Eq. 10. The dashed lines represent the predictions from the null model (Eq. 11). Right column: The difference between the observed asymptotic CM diffusion constants and the expected values from the null model, as  $\Delta D(p_m) = D(p_m) - (p_m D_{\text{RiAO}} + (1 - p_m) D_{\text{QTree}})$ . For better visualization across different system sizes, all data are normalized by  $D_{\text{QTree}}$ .

cases: the RiAO dynamics ( $p_m = 1$ ) and the dynamics of quenched trees ( $p_m = 0$ ). This raises the question of how this acceleration depends on the ring weight,  $N_m$ , and the mixing parameter,  $p_m$ .

For our mixing rule, Eq. (10), of the monomer Supplementary and node moves, the prediction of the null model, Eq. (11), reads  $D(p_m) = p_m D_{\text{RiAO}} + (1 - p_m) D_{\text{QTree}}$  or, equivalently,  $D(p_m)/D_{\text{QTree}} = 1 + (D_{\text{RiAO}}/D_{\text{QTree}} - 1)p_m$ . The panels in the left column of Fig. 7 show the corresponding results for the three types of investigated systems (ideal rings, self-avoiding rings and rings in melts) – note that the normalization to  $D_{\text{QTree}}$  allows us to show results for rings of different sizes on a common linear scale (Raw results of  $D$  are presented in Fig. ?? in the Supplementary Material.).

Results reveal the importance and character of deviations of the emergent dynamics from the null model. Namely, while the emergent dynamics in the melt is significantly accelerated and dominated by the deviations from the null model, the corrections appear to be more of a qualitative nature for self-avoiding rings and statistically insignificant for ideal rings. This said, our decision to normalize the diffusion constants in all three cases by those of the *asymptotically* faster Brownian Tree Dynamics (right column of Fig. 4) can lead to the wrong impression that  $D(p_m)$  extrapolates to zero for finite ring sizes (as it does indeed in the case of the slithering dynamics in

Fig. 9(d)). However, in the present case  $D(p_m)/D_{\text{QTree}}$  remains finite for all  $N_m$ , albeit much smaller than unity for ideal and self-avoiding double-folded rings and equal to zero only in the limit of infinite chain length.

In the right column of Fig. 7, we show the difference  $\Delta D(p_m) = D(p_m) - (p_m D_{\text{RiAO}} + (1 - p_m) D_{\text{QTree}})$  between the observed asymptotic CM diffusion constant and the expected value from the null model. To simplify a comparison with the data shown in the panels in the left column, we do not show absolute values for  $\Delta D(p_m)$  but  $\Delta D(p_m)/D_{\text{QTree}}$ . If  $\Delta D(p_m)$  vanishes by construction in the two limits  $p_m = 0$  and  $p_m = 1$  (i.e., a value of zero is in this case a “true” and not just an apparent zero), our data suggest an intriguing symmetry in how the node and the monomer dynamics combine.

The most general admissible expression for contributions  $\Delta D_{AB}$  to the ring CM diffusion constant,  $D$ , arising from a *coupling* of two distinct  $A$ - and  $B$ -types of dynamics would seem to be a sum of the form

$$\begin{aligned} \Delta D_{AB}(p_A, p_B) \\ = \sum_i a_i \left( (p_A D_A)^{\alpha_i} (p_B D_B)^{1-\alpha_i} \right)^{\beta_i} (p_A D_A + p_B D_B)^{1-\beta_i} \end{aligned} \quad (12)$$

with exponents  $0 \leq \alpha_i$ , assuring that (i)  $\Delta D_{AB} \neq 0$  if and only if both types of the elementary dynamics are present, (ii)  $\Delta D_{AB}$  has the same units as  $D_A$  and  $D_B$ , and (iii) the coupled dynamics is slowed down by the same factor as the  $A$ - and the  $B$ -dynamics, when both types of moves are rejected with equal probabilities,  $p_A = p_B = p$ :

$$\begin{aligned} \Delta D_{AB}(p_A = p, p_B = p) \\ = \sum_i a_i \left( (p D_A)^{\alpha_i} (p D_B)^{1-\alpha_i} \right)^{\beta_i} (p D_A + p D_B)^{1-\beta_i} \\ = p \sum_i a_i \left( D_A^{\alpha_i} D_B^{1-\alpha_i} \right)^{\beta_i} (D_A + D_B)^{1-\beta_i} \\ = p \Delta D_{AB}(p_A = 1, p_B = 1) \end{aligned} \quad (13)$$

Interestingly, our results for  $\Delta D_{AB}$  reported in the right column of Fig. 7 suggest that the coupling contribution adopts the simplest possible form of

$$\Delta D_{AB} \propto \sqrt{p_A D_A p_B D_B}. \quad (15)$$

Is this (in hindsight) obvious and inevitable or, alternatively, does our observation constrain the choice of admissible microscopic coupling mechanisms? Since the CM diffusion of our rings is diffusive in the long time limit, we consider as the simplest model the coupling of two diffusion steps,  $\vec{\delta}_A$  and  $\vec{\delta}_B$ , for a particle moving under the influence of two random processes  $A$  and  $B$ . To define the additional displacement,  $\vec{\delta}_{AB} = \delta_{AB} \hat{\delta}_{AB}$ , due to the coupling of the two steps, we need to specify its magnitude  $\delta_{AB} \equiv \|\vec{\delta}_{AB}\|$  and direction,  $\hat{\delta}_{AB} \equiv \vec{\delta}_{AB}/\|\vec{\delta}_{AB}\|$ . For the magnitude, admissible combinations of  $\delta_A$  and  $\delta_B$  have

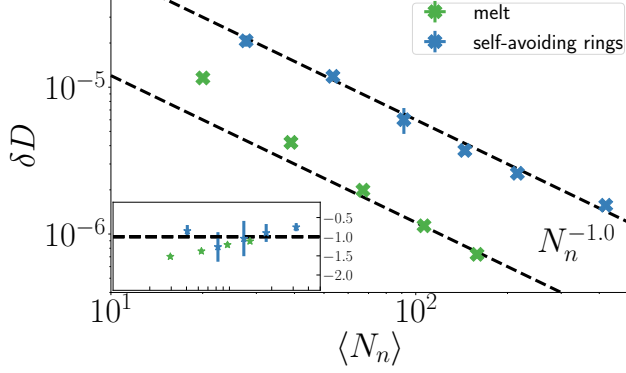


FIG. 8. Scaling behavior of the coupling contribution  $\delta D$  in Eq.16, extracted from fits of  $\Delta D_{AB}(N_n)$  to the functional form  $\delta D_{AB}(N_n)\sqrt{p_A p_B}$ . The data suggests a Rouse-like scaling  $\delta D(N_n) \sim N_n^{-1}$  for isolated self-avoiding rings, while the behavior for rings in the melt state exhibits a slow crossover towards a similar scaling.

to obey the same dimensionality constraint, that we have discussed above for the diffusion constant. With simple vector operations like  $\|\vec{\delta}_A \times \vec{\delta}_B\|$  and  $\vec{\delta}_A \cdot \vec{\delta}_B$  having the unit of the square of a length, one arrives rather naturally at a scaling,  $\delta_{AB} \propto \sqrt{\delta_A \delta_B}$ , of the length of the coupling steps with the geometric mean of the elementary step lengths, that may be modulated by geometric factors. On first sight, this seems to directly lead to the observed scaling  $\Delta D_{AB} = \langle \delta_{AB}^2 \rangle \propto \sqrt{\langle \delta_A^2 \rangle \langle \delta_B^2 \rangle} \propto \sqrt{D_A D_B}$  of the coupling contribution to the diffusion constant. However, the relation  $\Delta D_{AB} \equiv D_{AB} - D_A - D_B$  only holds, if additionally  $\hat{\delta}_{AB} = (\vec{\delta}_A \times \vec{\delta}_B) / \|\vec{\delta}_A \times \vec{\delta}_B\|$  or if the direction of the coupling steps,  $\hat{\delta}_{AB}$ , is not correlated with  $\vec{\delta}_A$  and  $\vec{\delta}_B$ . In contrast, if  $\hat{\delta}_{AB}$  lies in the plane spanned by the elementary steps,  $\vec{\delta}_A$  and  $\vec{\delta}_B$ , correlations lead to more complicated relations of the general type Eq. (12).

As our final point, Fig. 8 addresses the ring size dependence of the magnitude of  $\Delta D_{AB}$  arising from the coupling of the Brownian tree and the ring-in-an-array-of-obstacles-like dynamics. In spite of the vast difference in the amplitude of the Brownian tree dynamics for isolated self-avoiding rings and for rings in a melt (Fig. 4), the absolute magnitude of the CM motion due to the coupling with the RiAO-like dynamics is quite similar for the two systems. Our data for isolated self-avoiding rings are in good agreement with a Rouse-like scaling,  $\Delta D_{AB} \sim N^{-1}$ . Our data for melts are less clear, but like the diffusion constants measured for pure Brownian tree dynamics, they are compatible with a slow crossover to a Rouse-like scaling. Notably the total CM diffusion constant

$$D_{AB} = p_A D_A + p_B D_B + \delta D_{AB} \sqrt{p_A p_B} \quad (16)$$

in the melt case seems to be dominated asymptotically by the mobility arising from the coupling of the Brownian tree and the RiAO-like dynamics.

## VI. SUMMARY AND CONCLUSION

Ring polymers pose a number of challenging fundamental problems in polymer physics. In this article, we have studied the possible dynamics of a (lattice) model of tightly double-folded chains [1–3, 6, 24]. If the long-time goal is to apply the model to specific examples from a wide range of ring polymer systems (see e.g. [8, 12–18]), our objective here was to study generic aspects of the coupling of different local modes of dynamics. In particular, we have exploited the opportunity inherent in a mesoscale description to freely vary the relative kinetic rates instead of being limited to ratios emerging in particular experimentally or numerically accessible target or model systems.

Specifically, we have reimplemented and generalized our earlier elastic lattice model for tightly double-folded ring polymers [24]. To this end, we have extended the model such that sets of compatible ring and tree degrees of freedom are now simultaneously updated and defined at all moments of time. Then, we have introduced tree node moves complementing the original ring monomer moves. In addition to the spontaneous creation and deletion of side branches and the diffusive local mass transport along the tree, the present extension allows for a spatial diffusion of the tree that preserves the secondary structure of the double-folded rings.

We have explored the dynamics of tree-like polymer structures for three paradigmatic types of double-folded ring systems: ideal rings, isolated self-avoiding rings, and rings in the melt state. For the corresponding (combinations of) local moves, we have observed the expected signatures of the slithering of rings around the tree arising from the local transport of reptons, the ring-in-an-array-of-obstacles dynamics emerging from the additional possibility to absorb and grow side branches, and a Rouse-like dynamics due to the diffusion of tree nodes. In this respect, the dynamics of quenched trees in the melt state is particularly interesting. While the monomer diffusion is in almost perfect agreement with the expectation  $g_1 \sim t^{0.4}$  from the Rouse model for crumpled rings, there are also clear indications for a slow-down of the center-of-mass dynamics on intermediate scales. In particular, we have observed and analyzed a non-trivial dynamics emerging from the coupling of our ring monomer and tree node moves, which appears to asymptotically dominate the ring dynamics. At least qualitatively, the observed scaling of  $\Delta D_{AB} \sim N^{-1}$  is compatible with the interpretation that the constraint release due to the annealing of the tree structure can induce a Rouse-like dynamics.

We note that numerous experimental investigations using fluorescent microscopy have explored the 3D dy-

namics of chromatin in cell nuclei of mammals [49–52], drosophila [53, 54], and yeast [55]. Additionally, studies on genome dynamics within bacterial nucleoid have been conducted [56–59]. Many experiments reveal a subdiffusive behavior characterized by an exponent close to 0.4:  $g_1 \sim t^{0.4}$ , which are compatible with the behavior of the present model. However, observations [60, 61] of exponents in the range of 0.5 – 0.6 beyond the entanglement or branching scale call for different explanations.

## VII. SIMULATION SOFTWARE

The simulation software is an open-source package, distributed under the GNU General Public License v3.0 and written in C++. It is available at [62]. All simulations were performed on CBPSmn computer cluster of ENS-Lyon.

## VIII. ACKNOWLEDGEMENT

We gratefully acknowledge the support of the Centre Blaise Pascal’s IT test platform at ENS de Lyon (Lyon, France) for facilities. The platform operates the SIDUS solution [63] developed by Emmanuel Quemener. We thank Angelo Rosa and Cedric Vaillant for valuable discussions, and Ali Farnudi for his technical support. IJ and RE acknowledge funding from CNRS 80 Prime (MIMIC project).

### Appendix A: Approximate solution of the null model for the dynamics resulting from independent additive contributions

Consider two dynamics,  $A$  and  $B$ , generating MSDs  $g_A(t)$  and  $g_B(t)$ , respectively. We are interested in the MSD  $g_{AB}(t)$  of mixed schemes, where the local degrees of freedom are updated by  $A$  and  $B$  moves with probabilities  $p_A$  and  $p_B$ , respectively, and where typically (but not necessarily)  $p_A + p_B = 1$ . Our objective below is to estimate the full time dependence of the emergent behavior for the null model of independent and additive contributions from the  $A$  and  $B$  dynamics.

On first sight, the proper generalization of Eq. (11) would seem to be

$$g_{AB}(t) = p_A g_A(t) + p_B g_B(t). \quad (\text{A1})$$

However, with  $\lim_{p_B \rightarrow 0} g_{AB}(t) = p_A g_A(t)$  this form in general does not reproduce the exactly known limit of  $\lim_{p_B \rightarrow 0} g_{AB}(t) = g_A(p_A t)$ : a pure scheme, where only a fraction  $p_A$  of moves is accepted, has no other effect than to reduce the effectively elapsed time by a corresponding factor. The ansatz

$$g_{AB}(t) = g_A(p_A t) + g_B(p_B t) \quad (\text{A2})$$

overcomes this limitation. But while it reduces to Eq. (11) for simple diffusion, it fails for bounded MSD like those of the monomers relative to the ring CM, where after a suitably delayed time any of our dynamic processes would be predicted to independently contribute an MSD of  $\lim_{t \rightarrow \infty} g_2(t) = 2\langle R_g^2 \rangle$ .

To arrive at an alternative formulation, we note that for our definition of the relaxation time,  $\tau_X = \langle R_g^2 \rangle / D_X$ , the null model suggests

$$\frac{1}{\tau_{AB}} = \frac{p_A}{\tau_A} + \frac{p_B}{\tau_B}. \quad (\text{A3})$$

Now consider

$$\frac{1}{t_{AB}(g)} = \frac{p_A}{t_A(g)} + \frac{p_B}{t_B(g)}, \quad (\text{A4})$$

where  $t_X(g) = g_X^{-1}(t)$  denotes the inverse function of  $g_X(t)$ , i.e. the time  $t$  required with dynamics  $X$  to reach an MSD of  $g$ .  $t_{AB}(g)$  defined by Eq. (A4) and its inverse function  $g_{AB}(t)$  are well-behaved in a number of limiting cases. For simple diffusion,  $g_X(t) \sim D_X t$  so that  $t_X(g) \sim g/D_X$ , Eq. (A4) reduces to Eq. (11). By construction,  $\lim_{p_B \rightarrow 0} t_{AB}(g) = t_A(g)/p_A$ : as accepting only a fraction  $p_A$  of the  $A$  moves has the effect to reduce the effectively elapsed time by a corresponding factor, the time  $t_{AB}$  required to reach a given MSD of  $g$  increases by a factor  $1/p_A$  relative to the time  $t_A$  required with the pure  $A$  dynamics. In particular, we thus find for the inverse function  $\lim_{p_B \rightarrow 0} g_{AB}(t) = g_A(p_A t)$  as required. Plausibly, if both processes reach  $g$  equally fast,  $t_A(g) = t_B(g)$ , then Eq. (A4) suggests that the time required by the mixed process

$$t_{AB}(g) = \frac{t_A(g) t_B(g)}{p_A t_B(g) + p_B t_A(g)} \quad (\text{A5})$$

reduces to  $t_{AB}(g) = t_A(g) = t_B(g)$  for arbitrary  $p_A + p_B = 1$ . In contrast, if one of the processes reaches  $g$  much faster than the other,  $t_A(g) \ll t_B(g)$ , then over a wide range of  $p_A$ -values  $t_{AB}(g) \approx \frac{t_A(g)}{p_A}$  is essentially given by the time required by the faster process divided by the probability to activate the corresponding moves in the combined dynamics. Note that this relation holds in particular, when the second process by itself never reaches  $g$  (i.e. when  $t_B(g) = \infty$ ) and that according to Eq. (A4) the mixed process cannot reach MSD, which none of the pure processes can reach individually ( $t_{AB}(g) = \infty$ , if  $t_A(g) = t_B(g) = \infty$ ).

### Appendix B: Comparison of the null model to simulation data for double-folded rings

Conveniently Eq. (A4) is almost trivial to implement from a practical point of view, since it is straightforward (i) to generate numerically evaluable functions  $t(g)$  and



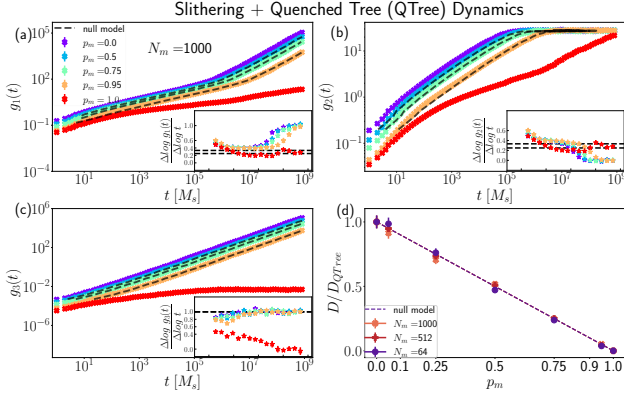


FIG. 9. MSDs for ideal double-folded rings, resulting from the combination of slithering dynamics and quenched tree dynamics, as a function of the mixing fraction  $p$  introduced in Eq. 10. Here,  $p_s$  denotes the fraction of slithering move in one MC sweep. The dashed gray lines in panels (a), (b), and (c) validate the null model using Eq. A4. Panel (d): the CM diffusion constant for the mixed dynamics across various chain lengths normalized by the diffusion constant pure QTree dynamics ( $p_{\text{slithering}} = 0$ ). Dashed lines represent the null model predictions for the corresponding chain lengths as described by Eq. 11.

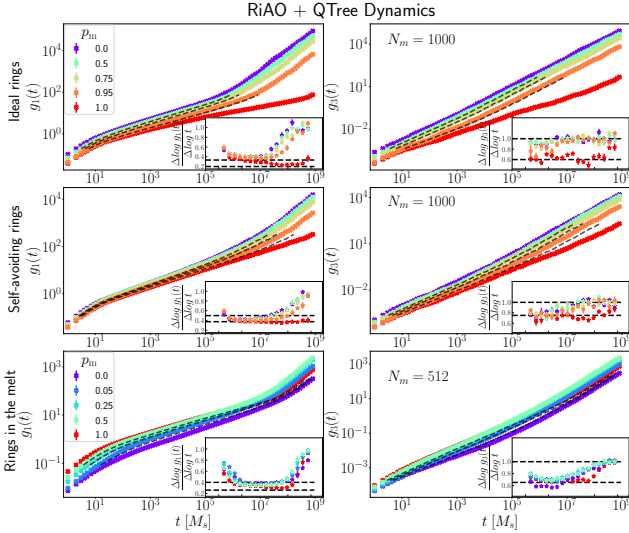


FIG. 10. MSDs resulting from the superposition of Quenched Tree (QTree) Dynamics and Ring-in-an-array-of-obstacles-like (RiAO) dynamics, based on the mixing fraction  $p_m$  introduced in Eq. 10.  $p_m$  represents the fraction of monomer move in one MC sweep and allows to interpolate between pure Ring-in-an-array-of-obstacles-like (RiAO) dynamics ( $p_m = 0$ ) and pure Quenched Tree Dynamics ( $p_m = 1$ ). Colored data points represent simulation data, while the thin gray lines indicate the predictions of the null model, Eq. A4, based on the simulation data for the pure case with  $p_m = 0$  and  $p_m = 1$ .

$g(t)$  from data sets associating paired values  $(t, g)$  us-

ing standard interpolation routines and (ii) to invert the position of the dependent and the independent variable in plotted graphs. We have tested Eq. (A4) for a case where we expect the null model to work: the dynamics emerging from the combination of repton and tree node moves, which are completely decoupled within our model. Panels (a)-(c) in Fig. 9 show  $g_1(t)$ ,  $g_2(t)$ , and  $g_3(t)$  for different proportions of repton and node moves, with  $0 \leq p_m \leq 1$ . Only accepted monomer moves are Repton moves, with  $q_{\text{rep}} = 1$ , and  $q_{\text{hp}} = 0$  (for more details, see Sec. IIID). For all considered values of  $p_m$  our simulation data (shown as colored symbols) are in excellent agreement with the lines representing corresponding estimates based on Eq. (A4) and our data for pure slithering and pure Brownian Tree Dynamics. Admittedly a bit trivially in the present case where  $D_{\text{Slithering}} = 0$ , the measured long time diffusion constants shown in Panels (d) also verify Eq. (11).

Figure 10 illustrates the results of the same analysis in the physically interesting case of an emergent dynamics to which monomer and node moves contribute in different proportions,  $0 \leq p_m \leq 1$  Eq. 10, such as to interpolate between pure Ring-in-an-array-of-obstacles-like (RiAO) dynamics ( $p_m = 1$ ) and pure Brownian Tree Dynamics ( $p_m = 0$ ). For non-interacting ideal rings, the predictions of the null model are again in excellent agreement with the simulation data (top row panels). For isolated self-avoiding rings (middle row panels), there are small, but noticeable deviation. Importantly, the accelerated dynamics of double-folded rings in a melt (bottom row panels) is clearly not described by the null model.

### Appendix C: The emergence of the ring-in-an-array-of-obstacles-like dynamics from the combination of hairpin and repton moves

To better understand possible signatures of non-trivial emergent dynamics arising from the interplay of two different local moves, we have modified the relative weight of Repton and Hairpin moves in the ring-in-an-array-of-obstacles-like dynamics (Fig. 11). Since neither Repton nor Hairpin moves are ergodic by themselves, the null model clearly does not apply:  $D_{\text{Rep}} = D_{\text{HP}} = 0$ , Eq. (A3) would predict  $D_{\text{RiAO}} = 0$ . And yet the rings move and equilibrate as long as *both* types of moves are present.

In particular, we observe the characteristic anomalous monomer and CM diffusion predicted by the ring-in-an-array-of-obstacles model equally well, when 99% of the Repton moves are suppressed as when 99% of the Hairpin moves are rejected (Panels (a)-(c) in Fig. 11). There is, however, a large quantitative difference in that suppressing 99% of the Hairpin moves has only a small effect on the relaxation time, while suppressing 99% of the Repton moves slows down the overall dynamics by a corresponding factor.

To analyse this situation, we denote as  $f_A$  and  $f_B$  the

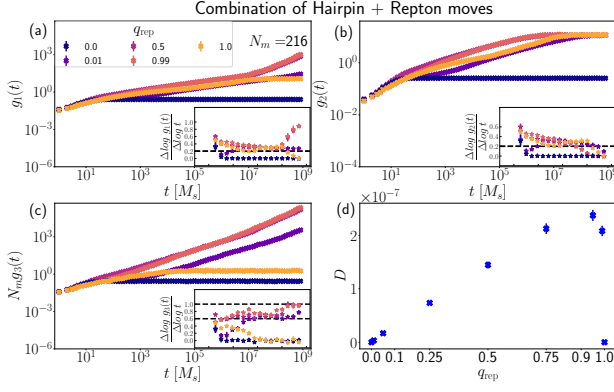


FIG. 11. The MSDs when modifying the relative weight of repton and hairpin move in the ring-in-an-array-of-obstacles-like (RiAO) dynamics. The Inset panel shows the local slopes of the data, and the horizontal dashed lines depict the expected behavior of RiAO dynamics. In Panel (D), the symbols represent CM diffusion constant.

fractions of accepted  $A$  (Repton) and  $B$  (Hairpin) type MC moves per sweep or unit of time; the remaining moves are rejected and do not contribute to the dynamics. Now suppose that  $a$  Repton moves and  $b$  Hairpin moves are required for an effective step of the ring-in-an-array-of-obstacles-like dynamics. The resulting fraction of RiAO moves,

$$f_{aA+bB} = \min\left(\frac{f_A}{a}, \frac{f_B}{b}\right), \quad (\text{C1})$$

generalizes to

$$f_{aA+bB} = \min\left(\frac{q_A f_A}{a}, \frac{q_B f_B}{b}\right), \quad (\text{C2})$$

if one changes the relative weight of Repton and Hairpin moves by accepting them only with reduced probabilities  $0 \leq q_A, q_B \leq 1$ .

Importantly,  $f_{aA+bB}$  is proportional to the asymptotic CM diffusion constant for the emergent coupled dynamics:  $D_{aA+bB} \sim f_{aA+bB}$ . For our choice of  $q_A = q$  and

$q_B = 1 - q$ , Eq. (C2) takes the simple form of two straight lines

$$f_{aA+bB} = \begin{cases} q \frac{f_A}{a} & \text{if } q < q^* \\ (1 - q) \frac{f_B}{b} & \text{if } q > q^* \end{cases} \quad (\text{C3})$$

originating at  $f_{aA+bB} \equiv 0$  for  $q = 0$  and  $q = 1$  and intersecting at  $q^* = af_B/(bf_A + af_B)$  where  $f_{aA+bB}(q)$  adopts its maximum value of  $f_{aA+bB}(q^*) = f_A f_B / (bf_A + af_B)$ .

The prediction is in good qualitative agreement with our simulation results shown in Fig. 11(d). The interpretation is straightforward. The existence of a maximum at finite  $0 < q = q^* < 1$  is indicative of a dynamics arising from a combination of moves. At the maximum  $\frac{q_B f_B}{b} = \frac{q_A f_A}{a}$ , so that Repton and Hairpin moves are attempted in “stoichiometric” proportions.  $q > q^*$  corresponds to  $\frac{q_B f_B}{b} < \frac{q_A f_A}{a}$ , where the limiting factor is the fraction of successful Hairpin moves. In the opposite case of  $q < q^*$  and  $\frac{q_B f_B}{b} > \frac{q_A f_A}{a}$  the combined dynamics is limited by the fraction of accepted Repton moves. The latter case corresponds to our simulations, where the vast majority of attempted monomer moves correspond to hairpin moves. In particular, the above analysis explains, why the frequent rejection of hairpin moves in our melts has such a small effect on the amplitude of the RiAO dynamics (Figure 4).

The effect of combining Repton and Hairpin moves thus seems at the same time spectacular and trivial. It is spectacular in that the emergent ring-in-an-array-of-obstacles-like dynamics is qualitatively completely different from what one observes in the two non-ergodic limiting cases of pure Hairpin or Repton moves: The rings become mobile and are able to anneal the connectivity of the trees characterizing the double-folding. But the way how the two moves combine appears to be as trivial as for the combination of hopping moves in the  $x$ - and  $y$ -directions on a square lattice in the case of a single particle diffusing along a tilted narrow strip. In particular, the particle remains localized, if it attempts to hop exclusively along one or the other of the axes of the lattice. And as in the case of our Repton and Hairpin moves, there is an optimal mixture of  $x$ - and  $y$ -moves, which in this example trivially depends on the orientation of the strip relative to the lattice.

- [1] A. Khokhlov and S. Nechaev, “Polymer chain in an array of obstacles,” *Physics Letters A*, vol. 112, no. 3, pp. 156 – 160, 1985.
- [2] M. Rubinstein, “Dynamics of ring polymers in the presence of fixed obstacles,” *Phys. Rev. Lett.*, vol. 57, pp. 3023–3026, 1986.
- [3] S. P. Obukhov, M. Rubinstein, and T. Duke, “Dynamics of a ring polymer in a gel,” *Phys. Rev. Lett.*, vol. 73, pp. 1263–1266, 1994.

- [4] A. Y. Grosberg, “Annealed lattice animal model and Flory theory for the melt of non-concatenated rings: Towards the physics of crumpling,” *Soft Matter*, vol. 10, pp. 560–565, 2014.
- [5] A. Rosa and R. Everaers, “Ring polymers in the melt state: The physics of crumpling,” *Phys. Rev. Lett.*, vol. 112, p. 118302, 2014.
- [6] J. Smrek and A. Y. Grosberg, “Understanding the dynamics of rings in the melt in terms of the annealed tree



- model,” *Journal of Physics: Condensed Matter*, vol. 27, no. 6, p. 064117, 2015.
- [7] J. Vinograd, J. Lebowitz, R. Radloff, R. Watson, and P. Laipis, “The twisted circular form of polyoma viral DNA,” *Proceedings of the National Academy of Sciences*, vol. 53, no. 5, pp. 1104–1111, May 1965.
  - [8] A. V. Vologodskii and N. R. Cozzarelli, “Conformational and thermodynamic properties of supercoiled DNA,” *Annual Review of Biophysics*, vol. 23, no. Volume 23, 1994, pp. 609–643, 1994.
  - [9] J. F. Marko and E. D. Siggia, “Statistical mechanics of supercoiled DNA,” *Phys. Rev. E*, vol. 52, pp. 2912–2938, 1995.
  - [10] H. Delius and A. Worcel, “Electron microscopic visualization of the folded chromosome of escherichia coli,” *Journal of Molecular Biology*, vol. 82, no. 1, pp. 107–109, 1974.
  - [11] R. Kavenoff and B. C. Bowen, “Electron microscopy of membrane-free folded chromosomes from escherichia coli,” *Chromosoma*, vol. 59, no. 2, pp. 89–101, Dec 1976.
  - [12] I. Junier, E. Ghobadpour, O. Espeli, and R. Everaers, “DNA supercoiling in bacteria: state of play and challenges from a viewpoint of physics based modeling,” *Front Microbiol*, vol. 14, p. 1192831, 2023.
  - [13] L. Liu and C. Hyeon, “Contact statistics highlight distinct organizing principles of proteins and RNA,” *Biophysical journal*, vol. 110, no. 11, pp. 2320–2327, June 2016.
  - [14] J. Kelly, A. Y. Grosberg, and R. Bruinsma, “Sequence dependence of viral RNA encapsidation,” *The Journal of Physical Chemistry B*, vol. 120, no. 26, pp. 6038–6050, 2016.
  - [15] S. W. Singaram, A. Gopal, and A. Ben-Shaul, “A prűfer-sequence based algorithm for calculating the size of ideal randomly branched polymers,” *The Journal of Physical Chemistry B*, vol. 120, no. 26, pp. 6231–6237, 2016.
  - [16] A. Rosa and R. Everaers, “Structure and dynamics of interphase chromosomes,” *PLOS Computational Biology*, vol. 4, no. 8, pp. 1–10, 2008.
  - [17] E. Lieberman-Aiden, N. L. van Berkum, L. Williams, M. Imakaev, T. Ragoczy, A. Telling, I. Amit, B. R. Lajoie, P. J. Sabo, M. O. Dorschner, R. Sandstrom, B. Bernstein, M. A. Bender, M. Groudine, A. Gnirke, J. Stamatoyannopoulos, L. A. Mirny, E. S. Lander, and J. Dekker, “Comprehensive mapping of long-range interactions reveals folding principles of the human genome,” *Science*, vol. 326, no. 5950, pp. 289–293, 2009.
  - [18] J. D. Halverson, J. Smrek, K. Kremer, and A. Y. Grosberg, “From a melt of rings to chromosome territories: the role of topological constraints in genome folding,” *Reports on Progress in Physics*, vol. 77, no. 2, p. 022601, Jan 2014.
  - [19] A. M. Gutin, A. Y. Grosberg, and E. I. Shakhnovich, “Polymers with annealed and quenched branchings belong to different universality classes,” *Macromolecules*, vol. 26, no. 6, pp. 1293–1295, 1993.
  - [20] M. Rubinstein, “Discretized model of entangled-polymer dynamics,” *Phys. Rev. Lett.*, vol. 59, pp. 1946–1949, 1987.
  - [21] A. Rosa and R. Everaers, “Conformational statistics of randomly branching double-folded ring polymers,” *The European Physical Journal E*, vol. 42, no. 1, p. 7, 2019.
  - [22] M. Doi and S. F. Edwards, *The Theory of Polymer Dynamics*. New York: Oxford University Press, 1986.
  - [23] T. Ge, S. Panyukov, and M. Rubinstein, “Self-similar conformations and dynamics in entangled melts and solutions of nonconcatenated ring polymers,” *Macromolecules*, vol. 49, no. 2, pp. 708–722, 2016.
  - [24] E. Ghobadpour, M. Kolb, M. R. Ejtehadi, and R. Everaers, “Monte carlo simulation of a lattice model for the dynamics of randomly branching double-folded ring polymers,” *Phys. Rev. E*, vol. 104, p. 014501, Jul 2021.
  - [25] J. D. Halverson, W. B. Lee, G. S. Grest, A. Y. Grosberg, and K. Kremer, “Molecular Dynamics simulation study of nonconcatenated ring polymers in a melt. I. Statics,” *The Journal of Chemical Physics*, vol. 134, no. 20, p. 204904, 2011.
  - [26] D. Michieletto, “On the tree-like structure of rings in dense solutions,” *Soft Matter*, vol. 12, pp. 9485–9500, 2016.
  - [27] B. H. Zimm and W. H. Stockmayer, “The dimensions of chain molecules containing branches and rings,” *J. Chem. Phys.*, vol. 17, pp. 1301–1314, 1949.
  - [28] P.-G. De Gennes, “Statistics of branching and hairpin helices for the dAT copolymer,” *Biopolymers*, vol. 6, p. 715, 1968.
  - [29] G. Parisi and N. Sourlas, “Critical behavior of branched polymers and the Lee-Yang edge singularity,” *Phys. Rev. Lett.*, vol. 46, pp. 871–874, 1981.
  - [30] J. Isaacson and T. C. Lubensky, “Flory exponents for generalized polymer problems,” *J. Physique Lett.*, vol. 41, pp. L469–L471, 1980.
  - [31] M. Daoud and J. F. Joanny, “Conformation of branched polymers,” *J. Physique*, vol. 42, pp. 1359–1371, 1981.
  - [32] R. Everaers, A. Y. Grosberg, M. Rubinstein, and A. Rosa, “Flory theory of randomly branched polymers,” *Soft Matter*, vol. 13, pp. 1223–1234, 2017.
  - [33] P. G. de Gennes, “Reptation of a polymer chain in the presence of fixed obstacles,” *The Journal of Chemical Physics*, vol. 55, no. 2, pp. 572–579, 1971.
  - [34] J. Qin and S. T. Milner, “Tube dynamics works for randomly entangled rings,” *Phys. Rev. Lett.*, vol. 116, p. 068307, Feb 2016.
  - [35] P.-G. De Gennes, *Scaling Concepts in Polymer Physics*. Ithaca: Cornell University Press, 1979.
  - [36] T. Ge, S. Panyukov, and M. Rubinstein, “Self-similar conformations and dynamics in entangled melts and solutions of nonconcatenated ring polymers,” *Macromolecules*, vol. 49, no. 2, pp. 708–722, 2016.
  - [37] T. C. B. McLeish, “Tube theory of entangled polymer dynamics,” *Advances in Physics*, vol. 51, no. 6, pp. 1379–1527, 2002.
  - [38] B. J. Gold, W. Pyckhout-Hintzen, A. Wischniewski, A. Radulescu, M. Monkenbusch, J. Allgaier, I. Hoffmann, D. Parisi, D. Vlassopoulos, and D. Richter, “Direct assessment of tube dilation in entangled polymers,” *Phys. Rev. Lett.*, vol. 122, p. 088001, Feb 2019.
  - [39] P. Malo de Molina, A. Alegría, J. Allgaier, M. Kruteva, I. Hoffmann, S. Prévost, M. Monkenbusch, D. Richter, A. Arbe, and J. Colmenero, “Direct observation of dynamic tube dilation in entangled polymer blends: A combination of neutron scattering and dielectric techniques,” *Phys. Rev. Lett.*, vol. 123, p. 187802, Nov 2019.
  - [40] K. E. Evans and S. F. Edwards, “Computer simulation of the dynamics of highly entangled polymers. part 1.—equilibrium dynamics,” *J. Chem. Soc., Faraday Trans. 2*, vol. 77, pp. 1891–1912, 1981.
  - [41] M. Newman and G. Barkema, *Monte Carlo Methods in*

- Statistical Physics*. Clarendon Press, 1999.
- [42] A. van Heukelum and G. T. Barkema, “Reaching large lengths and long times in polymer dynamics simulations,” *The Journal of Chemical Physics*, vol. 119, no. 15, pp. 8197–8202, 2003.
  - [43] V. Hugouvieux, M. A. V. Axelos, and M. Kolb, “Amphiphilic multiblock copolymers: From intramolecular pearl necklace to layered structures,” *Macromolecules*, vol. 42, no. 1, pp. 392–400, 2009.
  - [44] P. H. W. van der Hoek, A. Rosa, and R. Everaers, “Configurational entropy of tightly double folded ring polymers,” (*in preparation*).
  - [45] A. Rosa and R. Everaers, “Computer simulations of randomly branching polymers: Annealed versus quenched branching structures,” *Journal of Physics A: Mathematical and Theoretical*, vol. 49, no. 34, p. 345001, 2016.
  - [46] M. Kruteva, J. Allgaier, M. Monkenbusch, I. Hoffmann, and D. Richter, “Structure and dynamics of large ring polymers,” *Journal of Rheology*, vol. 65, no. 4, pp. 713–727, 07 2021.
  - [47] M. Kruteva, J. Allgaier, and D. Richter, “Topology matters: Conformation and microscopic dynamics of ring polymers,” *Macromolecules*, vol. 56, no. 18, pp. 7203–7229, 09 2023.
  - [48] M. Q. Tu, O. Davydovich, B. Mei, P. K. Singh, G. S. Grest, K. S. Schweizer, T. C. O’Connor, and C. M. Schroeder, “Unexpected slow relaxation dynamics in pure ring polymers arise from intermolecular interactions,” *ACS Polym Au*, vol. 3, no. 4, pp. 307–317, Aug 2023.
  - [49] I. Bronstein, Y. Israel, E. Kepten, S. Mai, Y. Shav-Tal, E. Barkai, and Y. Garini, “Transient anomalous diffusion of telomeres in the nucleus of mammalian cells,” *Phys. Rev. Lett.*, vol. 103, p. 018102, Jul 2009.
  - [50] F. M. Hameed, M. Rao, and G. V. Shivashankar, “Dynamics of passive and active particles in the cell nucleus,” *PLOS ONE*, vol. 7, no. 10, pp. 1–11, 10 2012.
  - [51] E. Kepten, I. Bronshtein, and Y. Garini, “Improved estimation of anomalous diffusion exponents in single-particle tracking experiments,” *Phys. Rev. E*, vol. 87, p. 052713, May 2013.
  - [52] A. Zidovska, D. A. Weitz, and T. J. Mitchison, “Micron-scale coherence in interphase chromatin dynamics,” *Proceedings of the National Academy of Sciences*, vol. 110, no. 39, pp. 15 555–15 560, 2013.
  - [53] W. Marshall, A. Straight, J. Marko, J. Swedlow, A. Dernburg, A. Belmont, A. Murray, D. Agard, and J. Sedat, “Interphase chromosomes undergo constrained diffusional motion in living cells,” *Current Biology*, vol. 7, no. 12, pp. 930–939, 1997.
  - [54] J. Vazquez, A. S. Belmont, and J. W. Sedat, “Multiple regimes of constrained chromosome motion are regulated in the interphase drosophila nucleus,” *Current Biology*, vol. 11, no. 16, pp. 1227–1239, 2001.
  - [55] G. G. Cabal, A. Genovesio, S. Rodriguez-Navarro, C. Zimmer, O. Gadal, A. Lesne, H. Buc, F. Feuerbach-Fournier, J.-C. Olivo-Marin, E. C. Hurt, and U. Nehrbass, “Saga interacting factors confine subdiffusion of transcribed genes to the nuclear envelope,” *Nature*, vol. 441, no. 7094, pp. 770–773, 2006.
  - [56] S. C. Weber, A. J. Spakowitz, and J. A. Theriot, “Bacterial chromosomal loci move subdiffusively through a viscoelastic cytoplasm,” *Phys. Rev. Lett.*, vol. 104, p. 238102, Jun 2010.
  - [57] —, “Nonthermal atp-dependent fluctuations contribute to the in vivo motion of chromosomal loci,” *Proceedings of the National Academy of Sciences*, vol. 109, no. 19, pp. 7338–7343, 2012.
  - [58] A. Javer, Z. Long, E. Nugent, M. Grisi, K. Siriwatwetchakul, K. D. Dorfman, P. Cicuta, and M. Cosentino Lagomarsino, “Short-time movement of E. coli chromosomal loci depends on coordinate and subcellular localization,” *Nature Communications*, vol. 4, no. 1, p. 3003, 2013.
  - [59] S. Subramanian and S. M. Murray, “Subdiffusive movement of chromosomal loci in bacteria explained by DNA bridging,” *Phys. Rev. Res.*, vol. 5, p. 023034, Apr 2023.
  - [60] D. B. Brückner, H. Chen, L. Barinov, B. Zoller, and T. Gregor, “Stochastic motion and transcriptional dynamics of pairs of distal DNA loci on a compacted chromosome,” *Science*, vol. 380, no. 6652, pp. 1357–1362, Jun 2023.
  - [61] P. Mach, P. I. Kos, Y. Zhan, J. Cramard, S. Gaudin, J. Tünnermann, E. Marchi, J. Eglinger, J. Zuin, M. Kryzhanovska, S. Smallwood, L. Gelman, G. Roth, E. P. Nora, G. Tiana, and L. Giorgetti, “Cohesin and ctf control the dynamics of chromosome folding,” *Nature Genetics*, vol. 54, no. 12, pp. 1907–1918, 2022.
  - [62] E. Ghobadpour, “Coarse-grain bacterial DNA simulator (CGBD),” Feb. 2025. [Online]. Available: <https://doi.org/10.5281/zenodo.14893438>
  - [63] E. Quemener and M. Corvellec, “Sidus—the solution for extreme deduplication of an operating system,” *Linux J.*, vol. 2013, no. 235, Nov. 2013.